

Automated Segmentation of Routinely Hematoxylin-Eosin–Stained Microscopic Images by Combining Support Vector Machine Clustering and Active Contour Models

Dimitris Glotsos, M.Sc., Panagiota Spyridonos, Ph.D., Dionisis Cavouras, Ph.D., Panagiota Ravazoula, M.D., Petroula-Arampantoni Dadioti, M.D., and George Nikiforidis, Ph.D.

OBJECTIVE: To develop a method for the automated segmentation of images of routinely hematoxylin-eosin (H-E)–stained microscopic sections to guarantee correct results in computer-assisted microscopy.

STUDY DESIGN: Clinical material was composed 50 H-E–stained biopsies of astrocytomas and 50 H-E–stained biopsies of urinary bladder cancer. The basic idea was to use a support vector machine clustering (SVMC) algorithm to provide gross segmentation of regions holding nuclei and subsequently to refine nuclear boundary detection with active contours. The initialization coordinates of the active contour model were defined using a SVMC pixel-based classification algorithm that discriminated nuclear regions from the surrounding tissue. Starting from the boundaries of these regions, the snake fired and propagated until converging to nuclear bound-

aries.

RESULTS: The method was validated for 2 different types of H-E–stained images. Results were evaluated by 2 histopathologists. On average, 94% of nuclei were correctly delineated.

CONCLUSION: The proposed algorithm could be of value in computer-based systems for automated interpretation of microscopic images. (Analyt Quant Cytol Histol 2004;26:000–000)

Keywords: computer-assisted diagnosis, automated segmentation, support vector machine clustering, active contour.

The nucleus is a very important structure within the cell as far as diagnosis of the severity of a tumor is

From the Medical Image Processing and Analysis Laboratory, Department of Medical Physics, School of Medicine, University of Patras, and Department of Pathology, University Hospital, Rio, Patras; Department of Medical Instrumentation Technology, Technological Education Institution of Athens; and Department of Pathology, General Anticancer Hospital METAXA, Piraeus, Greece.

Mr. Glotsos is -----, Medical Image Processing and Analysis Laboratory, Department of Medical Physics, School of Medicine, University of Patras.

Dr. Spyridonos is -----, Medical Image Processing and Analysis Laboratory, Department of Medical Physics, School of Medicine, University of Patras.

Dr. Cavouras is -----, Department of Medical Instrumentation Technology, Technological Education Institution of Athens.

Dr. Ravazoula is -----, Department of Pathology, University Hospital.

Dr. Dadioti is -----, Department of Pathology, General Anticancer Hospital METAXA.

Dr. Nikiforidis is -----, Medical Image Processing and Analysis Laboratory, Department of Medical Physics, School of Medicine, University of Patras.

The present research was funded by the Greek Ministry of Education and the European Union under research fund HRAKLEITOS—Development of New Machine Learning Methods for Medical Image Processing and Analysis Applications.

Address reprint requests to: Dimitris Glotsos, M.Sc., Medical Image Processing and Analysis Laboratory, Department of Medical Physics, University of Patras, 265 00 Rio-Patras, Greece (dimglo@med.upatras.gr).

Financial Disclosure: The authors have no connection to any companies or products mentioned in this article.

concerned. It has long been recognized that nuclei carry important information,¹ which, if quantified, can allow diagnosis and potentially prediction of the course of the disease.² Consequently, nuclear boundary detection and segmentation play an important role in computer-aided diagnosis and prognosis.

Nuclear boundary detection is not straightforward, especially when routinely stained microscopic images are involved. Among the various types, hematoxylin-eosin (H-E)-stained histologic images are considered the most difficult and problematic to process.³ H-E images present the greatest complexity due to variability in staining of nuclei and surrounding tissue.⁴ Additionally, the existence of spatially closely located nuclei complicates accurate detection of nuclear boundaries.

Previous approaches to cell and nuclei segmentation can be categorized into semiautomated (requiring user interactive participation) and automated methods. Semiautomated approaches have been designed to operate in conjunction with human screening^{5,6}; their performance has depended mainly on the establishment of a priori assumptions for nuclear morphology, spatial distribution and texture. Automated methods have investigated histogram-based techniques, edge detection methods, region-based algorithms, pattern recognition approaches and active contour models.⁷⁻¹⁵ Histogram-based techniques have been successful for images with uniform illumination.⁷ Edge detection algorithms have relied on the idea of detecting discontinuities of pixel intensities at the boundary of different objects.⁸ Region-based algorithms have assumed objects characterized by homogeneous intensity and have performed segmentation utilizing region growing, splitting and merging.⁹ Pattern recognition approaches have been established on the basis of supervised training of a classifier to discriminate between nuclei and background.¹⁰ However, edge detection and histogram-based methods are most sensitive to the presence of noise and artifacts.¹¹ Region-based algorithms are less sensitive to artifacts but have high computational complexity.⁹ H-E-stained images are considered among the most complex, noisy images and are characterized by great variability in staining intensity^{3,4}; thus, the aforementioned segmentation techniques are difficult to implement on H-E images.

Contour-based models are considered very promising for automated nuclear segmentation.¹²⁻¹⁵ The success of contour models depends mainly on

the initial assumptions made for nuclear morphology, the existence of subnuclear structures and mostly on the initialization condition of the deformable model¹⁵; the more accurate the initial estimation concerning nuclei boundaries, the better the contour model works. These limitations have restricted the application of active contours in nuclear segmentation of H-E images.

In the current approach, we propose a novel methodology for the automated segmentation of routinely H-E-stained microscopic images. The basic idea is to use a support vector machine clustering (SVMC) algorithm to provide gross segmentation of nuclear regions and subsequently to refine nuclear boundary detection with active contour models. SVMC is a state-of-the-art method that, until now, has not been examined beyond its theoretical foundation.¹⁷ The method was tested on 2 types of H-E nuclei images. The algorithm made no a priori assumptions about either size, shape, texture or spatial distribution of nuclei.

Materials and Methods

The clinical data were composed of 2 types of histologic material: (1) 50 H-E-stained biopsies of astrocytomas, and (2) 50 H-E-stained biopsies of urinary bladder cancer. The material was collected from the Department of Pathology, University Hospital of Patras, Patras, Greece. For each biopsy, a histopathologist (P.R.) specified the most representative region. From this region, images were acquired (768×576×8 bit) using a Zeiss Axiostar-Plus microscope (Zeiss, Wetzlar, Germany) connected to a Leica DC 300 F color video camera (Leica, Germany). The objective was a 40:1 planachromat with N.A. 0.65. The intensity (gray level) of each pixel in the digitized image refers to the measured light intensity transmitted through the sample.

SVMC Methodology for Estimating the Starting Position of the Active Contour Model

The initialization coordinates, or search space, of the active contour model, or snake, were defined by using an SVMC pixel-based classification algorithm that separated nuclear regions from the surrounding tissue. Starting from the boundaries of these regions, the snake fired and propagated until converging to nuclear boundaries. The gross estimation of nuclear regions was initialized by (1) assigning to each image pixel a 5-dimensional textural vector, and (2) subsequently searching in the feature space for clusters that corresponded to nuclei

and surrounding tissue using an SVMC algorithm.

Feature Generation. Each image was initially scanned by a 5×5 pixel window $I(x,y)$, with x,y image rows and columns. At every position of the window, the center pixel was assigned a 5-dimensional feature vector $x_i = \{f_j\}$, where $i = (1, \dots, N)$, with $N=5$ the number of image pixels and $j = (1, \dots, 5)$ the number of features. Generated features were the following:

1) The energy of the first and second detailed images of the Mallat nonorthogonal discrete wavelet transform¹:

$$f_{1,2} = \frac{1}{MN} \sum_{x,y} (D_{s,1,2}(x,y))^2, \quad (1)$$

where D_s is the nonorthogonal discrete wavelet transform¹⁶ of the 5×5 image window I , $s=2$ the wavelet scale, $M=1, \dots, x$ image rows, $N=1, \dots, y$ image columns and $f_{1,2}$ the energy of the first and second detailed images. The usefulness of the wavelet Mallat transform in chromatin texture description has already been highlighted in the literature.¹

2) The spread $S(1,1)$ and cross relation $S(2,2)$ of the autocorrelation function¹⁸ for all possible displacements m, n inside the 5×5 window (equations 2–6). The efficacy of these features in nuclei segmentation has been reported.¹⁰

$$f_3 = \sum_{m=0}^5 \sum_{n=-5}^5 (m-n_m)(n-n_n) A_F(m, n), \quad (2)$$

and

$$f_4 = \sum_{m=0}^5 \sum_{n=-5}^5 (m-n_m)^2 (n-n_n)^2 A_F(m, n), \quad (3)$$

where,

$$n_m = \sum_{m=0}^5 \sum_{n=-5}^5 m A_F(m, n), \quad (4)$$

$$n_n = \sum_{m=0}^5 \sum_{n=-5}^5 n A_F(m, n), \quad (5)$$

and

$$A_F(m, n) = \sum_j \sum_k F(j, k) F(j-m, k-n). \quad (6)$$

3) A new feature was developed for the purposes of the present study; it was based on the Parzen estimation technique.¹⁹ The Parzen-based homogeneity feature (PBH) was calculated according to equation 7:

$$f_5 = PBH = \sum_{i=1}^{N-1} \exp\left(-\left(\frac{d \cdot 0.8326}{\sigma}\right)^2\right), \quad (7)$$

where d is the Mahalanobis distance, N is the total number of window pixels, and σ is a smoothing parameter. The Mahalanobis²⁰ distances d of the gray level value of the center pixel from the gray level values of the rest 24 pixels inside the 5×5 window were computed. The resulting Mahalanobis distances were then passed through a radial basis function (RBF) kernel and summed to give an estimation of the gray level probability density function inside each 5×5 window. The value that resulted after the summation of all exponentiated Mahalanobis distances was assigned to the center pixel. By using the RBF kernel, the most “probable” gray level value of the center pixel was calculated based on the information obtained from the center pixel’s neighbors (i.e., the gray level values of the rest 24 pixels inside each window). The optimum setting for σ was experimentally determined to be equal to 0.06 after testing values ranging from 0.005 to 10.

PBH is a new feature we propose for encoding information on local pixel inhomogeneities. Pixel windows with similar intensity values give high values for PBH. When inhomogeneities are detected (i.e., boundaries), the feature takes low values.

Feature Clustering. Following feature generation, all feature vectors x_i were inputted to a SVMC algorithm that clustered the data into partitions corresponding to different nuclei and surrounding tissue regions. The basic idea behind the SVMC is detailed elsewhere.¹⁷ Input data x_i were initially transformed into a higher-dimensional feature space via a Gaussian RBF mapping kernel with optimum value for σ , experimentally determined equal to $\sigma=0.5$ (equation 8).

$$K_{RBF}(x, x_i) = \exp\left(-\frac{\|x-x_i\|^2}{2\sigma^2}\right). \quad (8)$$

In that feature space the machine seeks the minimum data enclosing sphere that encircled all input vectors. Based on the above concept, we calculated the sphere radius R as follows¹⁷:

$$R^2(x) = K(x, x) - 2 \sum_j \beta_j K(x_j, x) + \sum_{ij} \beta_i \beta_j K(x_i, x_j), \quad (9)$$

where K is the RBF kernel, β are Lagrange multipliers, x_i are the original data points, and x_j are the images of the points to the transformed feature space. By mapping the sphere back onto the original fea-

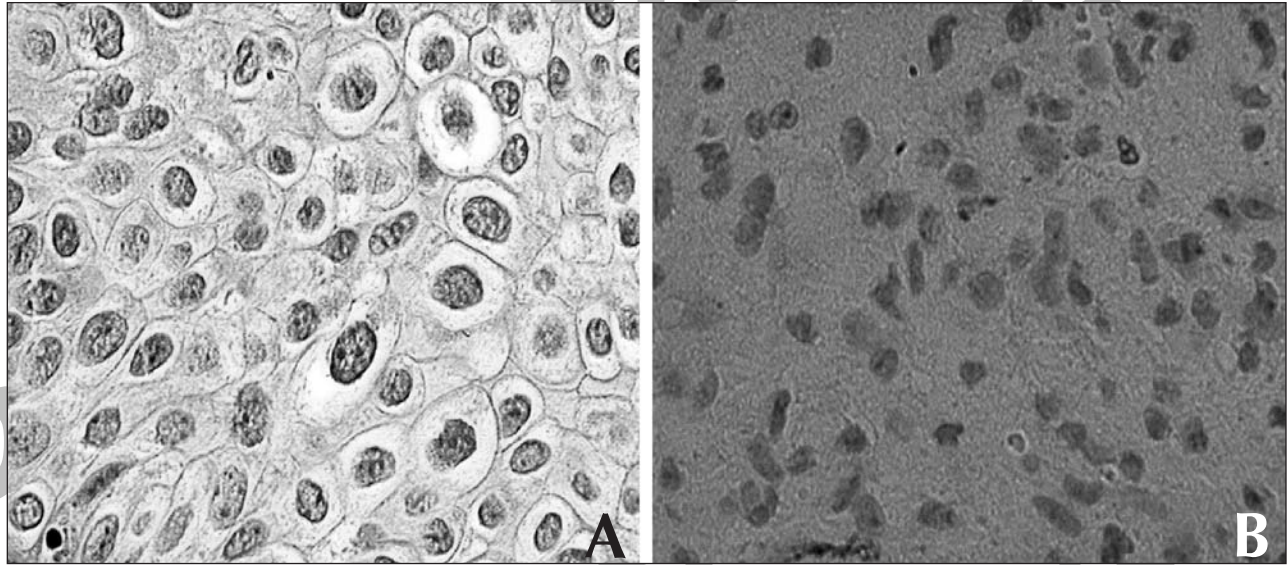


Figure 1 (A) H-E-stained image of urinary bladder cancer. (B) H-E-stained image of astrocytomas (A and B, $\times 400$).

ture space (Figure 2), the sphere broke down into several contours that surrounded different clusters of data. This mapping was achieved by employing the commercially available MATLAB code package proposed by Ben Hur et al.^{17,21}

After applying the SVMC algorithm, data were partitioned into several clusters, as illustrated in Figure 2. In order to identify which of these clusters corresponded to nuclei, the following procedure had been carried out: initially, 300 random nuclei were sampled from 10 images. From these nuclei, a 5-dimensional feature vector $\{f_1, \dots, f_5\}$ was extracted, as described below. The mean vector of the 300 generated nuclei feature vectors was calculated and regarded as the average nuclear cluster centroid c_0 (Figure 3). Subsequently, the cluster centroids c_i for each image (im_j) were computed; where $i = \{1, \dots, M\}$, M is the number of clusters that resulted from the SVMC algorithm, $j = \{1, \dots, N\}$, and $N = 100$ is the total number of images. Examining each im_j separately, all cluster centroids c_i were compared to the average sampled nuclear cluster center c_0 (Figure 3). The c_i closest to c_0 was considered the nuclei cluster centroid c_{nuclei} and the remainder considered background. Following that, a binary image was created by setting to white (gray level value 255) only those pixels that corresponded to c_{nuclei} . The remaining pixels were considered background and were set to black (gray level value 0) (Figure 4). The resulted binary images were further processed for the elimina-

tion of small, noisy regions by means of size filtering and fill-holes operations (Figure 5).²² By applying edge detection mask filters as proposed by Gonzalez,²³ only boundaries were retained (Figure 6) and subsequently superimposed on the original images (Figure 7).

Active Contour Model for the Final Localization of Nuclear Boundaries

Active contour algorithms are designed to detect boundaries around objects by generating curves (snakes) that can be deformed based on information offered by the objects themselves. In this work the gradient vector flow (GVF) model was utilized.²⁴ Each nucleus was processed separately. The snake originated at image coordinates previously defined based on an estimation by the SVMC algorithm. Subsequently the snake was deformed according to the effect of external forces. These were computed as a function of the spatial and directional distribution of the gradient vectors of a gray level image.²⁴ The active contour model is given in 11:

$$x_t(s,t) = ax''(s,t) - bx'''(s,t) + v. \quad (11)$$

$x_t(s,t)$ is the snake curve, with s ranging from 0 to 1, and t is time; a and b are weight parameters that control the snake's tension and rigidity, respectively. x'' and x''' are second and third derivatives of $x_t(s,t)$, and v is the gradient vector flow external

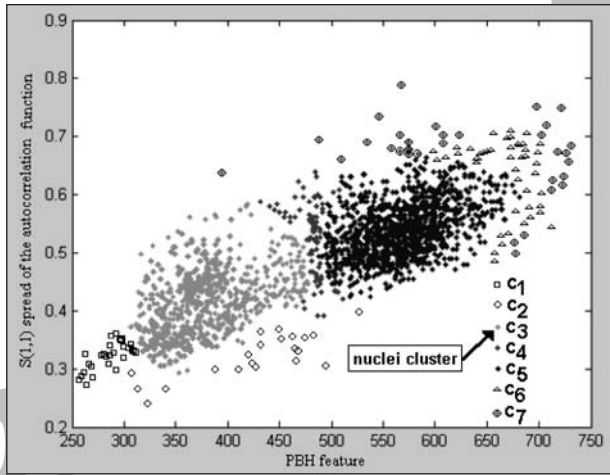


Figure 2 Two-dimensional clustering results of the SVMC algorithm for the H-E-stained image of urinary bladder cancer shown in Figure 1.

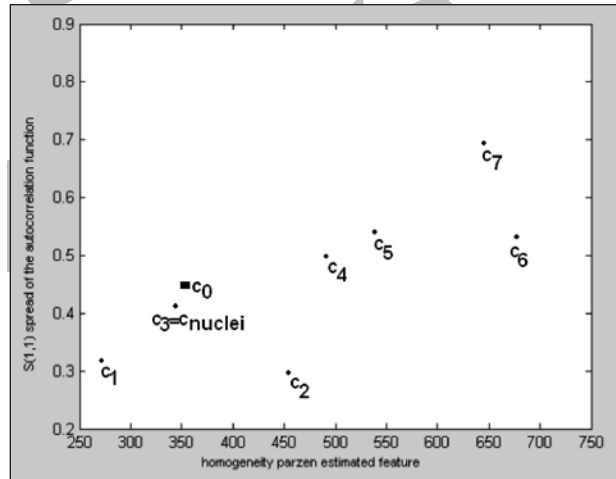


Figure 3 Identification of the cluster center c_i that corresponds to nuclei cluster for the H-E-stained image of urinary bladder cancer illustrated in Figure 1. The c_i closest to c_0 is considered the cluster centroid of nuclei and the remaining clusters considered background.

force field defined by equations 12 and 13.

$$v = E_{ext}^i(x,y), \tag{12}$$

and

$$E_{ext}^1(x,y) = -|\nabla I(x,y)|^2, \tag{13}$$

where $I(x,y)$ is the gray level image, and E_{ext}^1 is the external energy that leads the snake towards edges.

Parameters a and b were experimentally determined as equal to 0.05 and 0.1, respectively. By the effect of these forces, the snake propagated until it converged to nuclear boundaries (Figure 8). To realize this algorithm we utilized the GVF MATLAB toolbox, available from Lee et al.²⁵

Evaluation of Segmentation Results

The most reliable method proposed so far for eval-

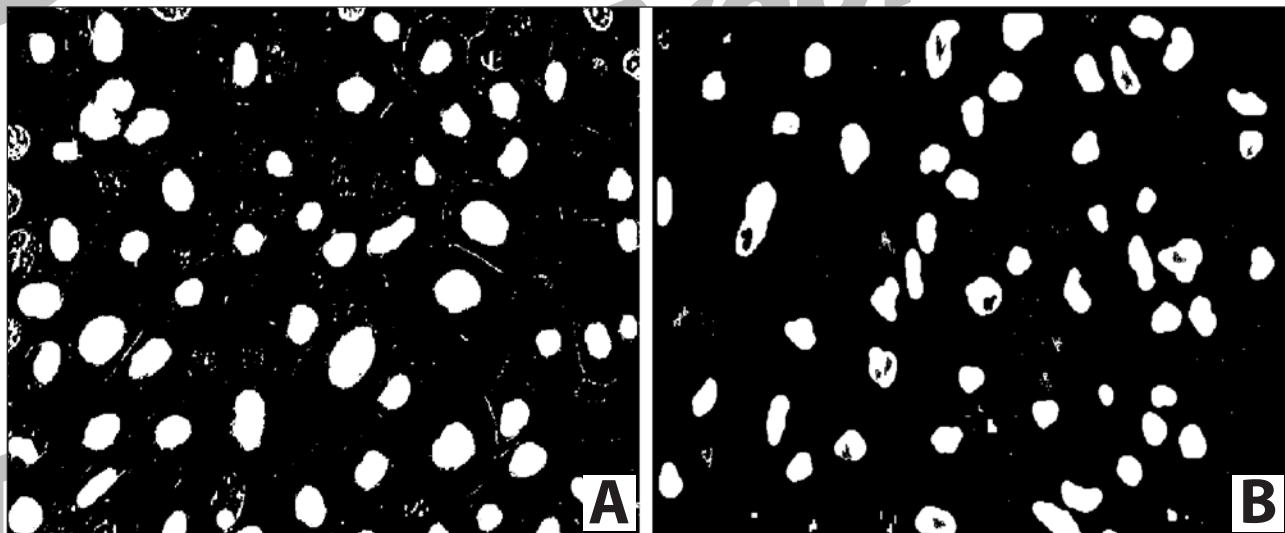


Figure 4 Initial estimation of nuclei and surrounding tissue regions by the SVM clustering algorithm. (A) Results for the H-E-stained image of urinary bladder cancer illustrated in Figure 1. (B) H-E-stained image of astrocytoma shown in Figure 1.

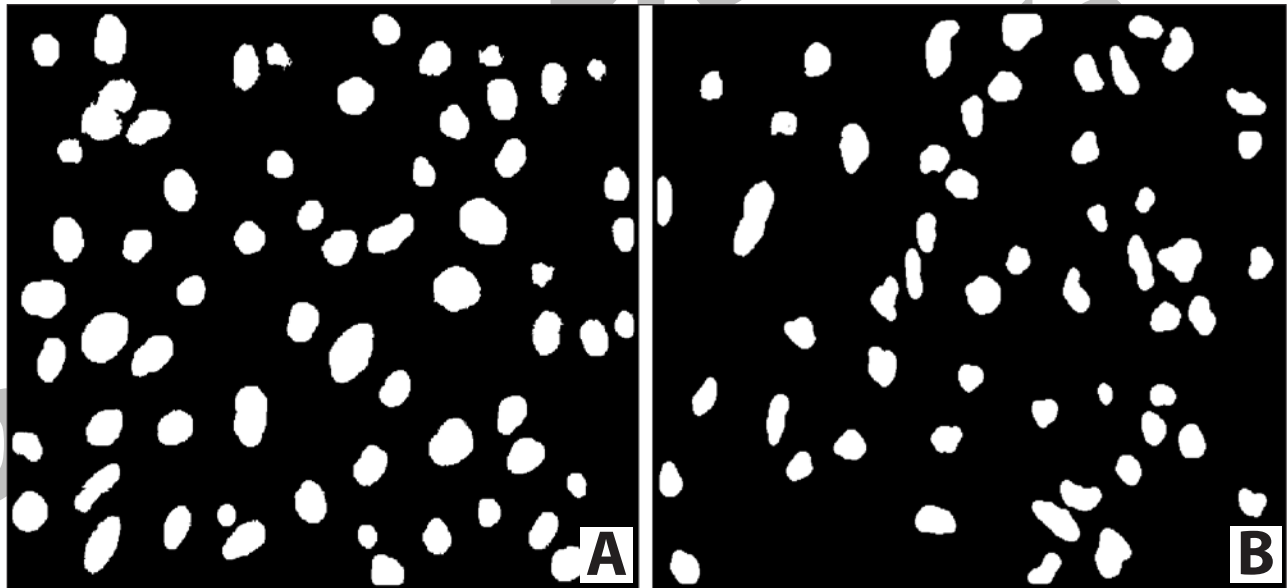


Figure 5 Corrected binary images for elimination of small, noisy regions with fill holes and size filtering. (A) Results for the H-E-stained image of urinary bladder cancer illustrated in Figure 1. (B) H-E-stained image of astrocytoma shown in Figure 1.

uating the performance of nuclear segmentation algorithms has been to compare results against those of manual segmentation by histopathologists.¹³ By visually inspecting each pair of original and segmented images, 2 histopathologists (P.R. and P.D.) assessed the success of the segmentation algorithm

by noting those nuclei that were correctly outlined. As a quantitative measure of the success of the segmentation algorithm, we used a measure of segmentation accuracy¹⁴—that is, the likelihood that a segmented object is an actual nucleus and is correctly circumscribed:

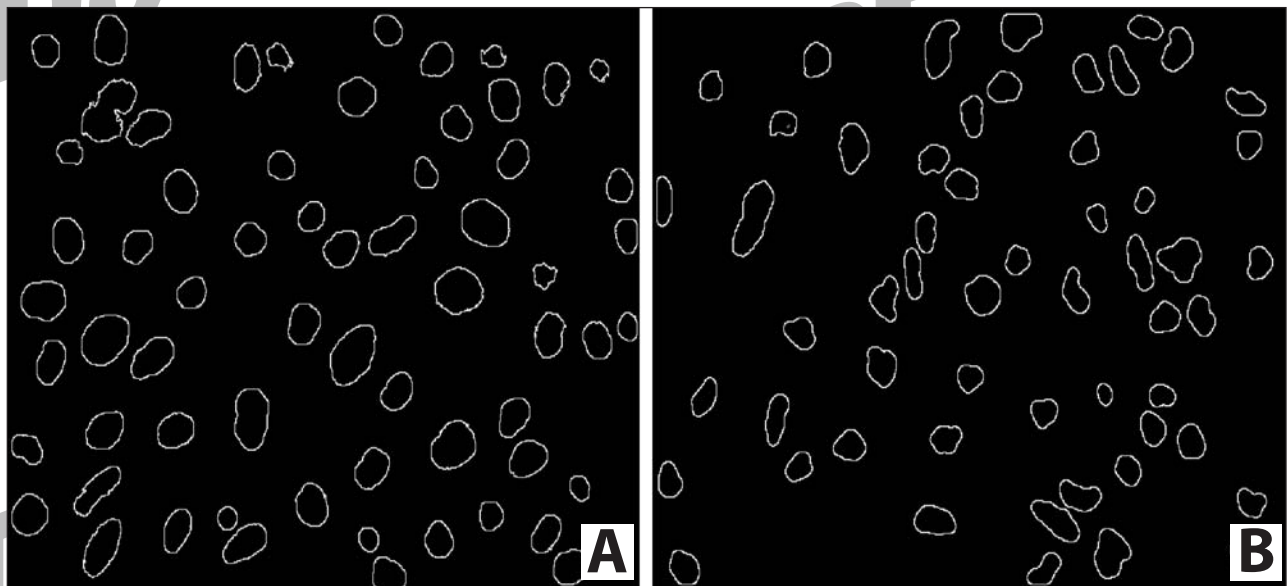


Figure 6 Edge detection using edge detection filtering. (A) Results for the H-E-stained image of urinary bladder cancer shown in Figure 1. (B) H-E-stained image of astrocytoma shown in Figure 1.

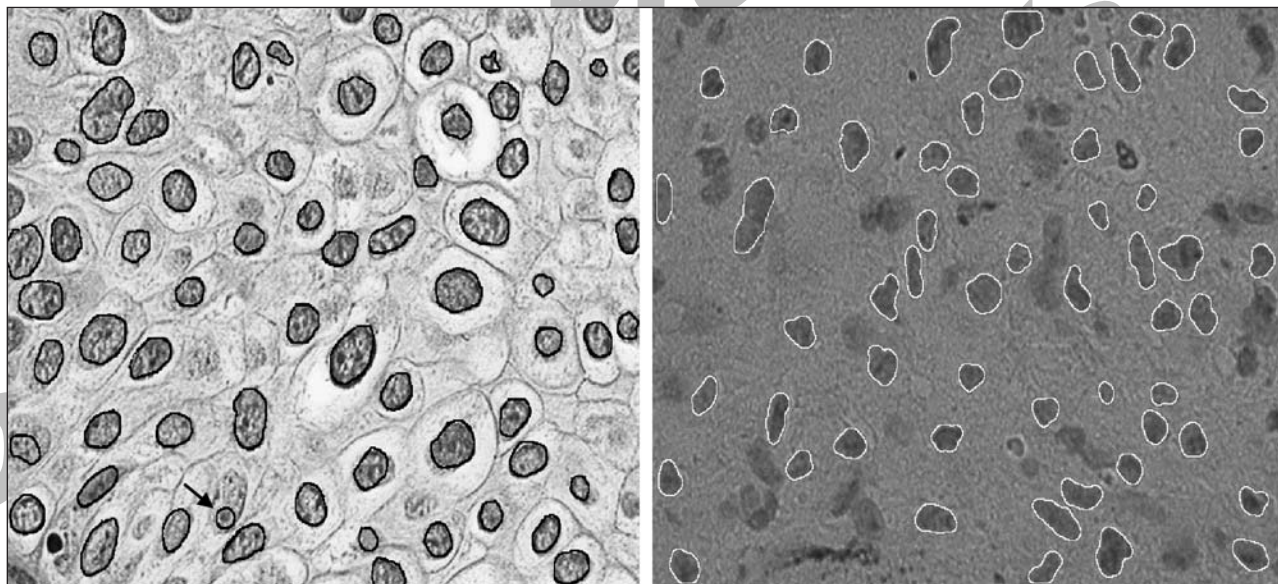


Figure 7 Edge estimation superimposed on the original image. The coordinates of nuclear boundaries constitute the initialization condition for the snake model. Arrow indicates incorrectly segmented nuclei.

$$Accuracy = \frac{TP}{TP+FN} \quad (14)$$

where TP are those nuclei that have been correctly identified by the segmentation algorithm and FN those nuclei erroneously or inadequately delineated. The results are indicated in Table I.

Results

The segmentation algorithm was applied to 50 H-E-stained images of astrocytomas and 50 H-E-stained images of urinary bladder cancer. On average, 94% of nuclei were correctly identified whatever their spatial configuration (isolated,

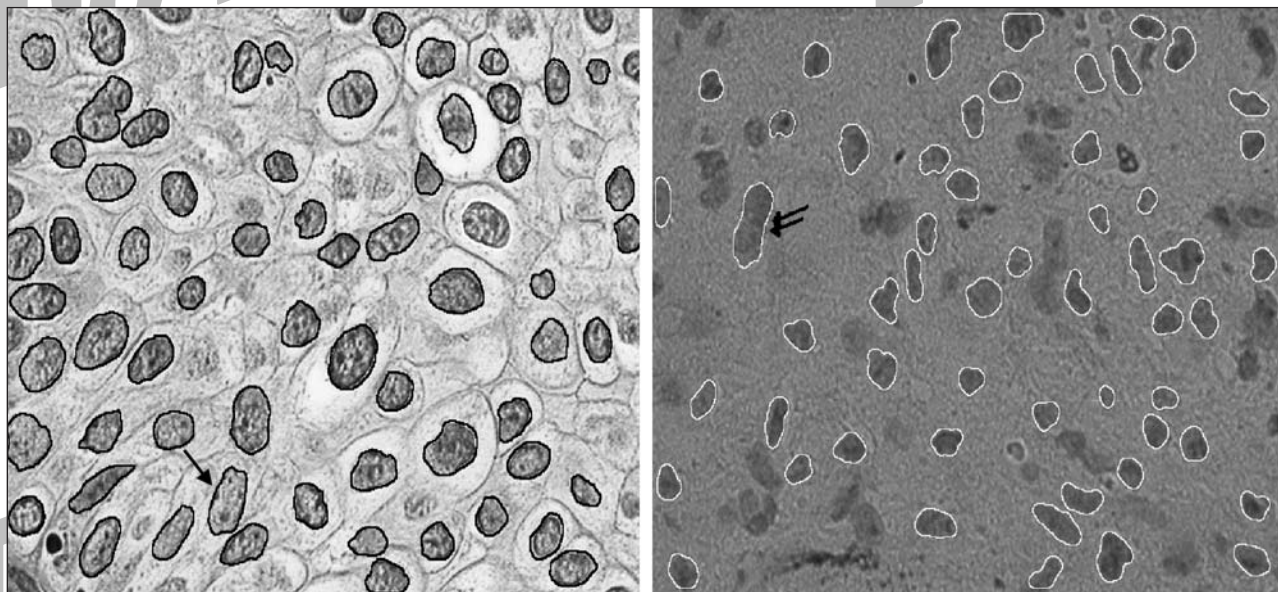


Figure 8 GVF active contour model activates and propagates to locate final nuclear boundaries. Arrow indicates correctly segmented nuclei as compared to Figure 5. Double arrow indicates 2 overlapping nuclei erroneously recognized as a single nucleus.

Table I Segmentation Results According to the Histopathologists' Evaluation in Terms of Correctly and Incorrectly Delineated Nuclei

Expert	Type of microscopic image	Correctly delineated nuclei (%)	Segmentation errors due to fused and/or overlapping nuclei (%)	Segmentation errors for other reasons (%)
P.R.	H-E astrocytomas	95	3	2
	H-E urinary bladder cancer	96	2	2
P.D.	H-E astrocytomas	93	3	4
	H-E urinary bladder cancer	92	4	4
Average accuracy	H-E astrocytomas	94	3	3
	H-E urinary bladder cancer	94	3	3
Total average accuracy		94	3	3

touching, overlapping, corrupted). The results of the segmentation process for each expert on every type of microscopic image tested are presented in Table I.

Discussion

Segmentation of microscopic images has been an active field of investigation for the past 30 years. Studies by Giaretti,³³ Rodenacker,³⁴ Aubele³⁵ and Brenner³⁶ were pioneering efforts in the field of computer-based image analysis in cytopathology and histopathology. The most recent efforts that aimed at automated nuclear segmentation have reported promising rates of "acceptable" segmentation, such as 80%,¹³ approximately 85%,²⁶ 89%,²⁷ 98.3%²⁸ and 99%.¹⁵ In the present study, nuclear segmentation accuracy reached approximately 94%. The results may be regarded as most encouraging considering that the H-E staining protocol employed in this study is not as accurate in labeling nuclei as are other, specialized staining protocols evaluated in previous studies.^{6,11-15,26-28} Fine needle aspiration images were utilized,^{13,14} as were Papanicolaou-stained cervical images.^{6,15} Crocker and Nar stained cervical images,¹¹ enhancing contrast among nuclei and background and thus simplifying the segmentation task.^{4,15} H-E images do not offer such attractive features because they offer great variability in staining intensity.³⁰ Despite these drawbacks, the H-E complex is the one adopted in daily clinical practice due to the simplicity in preparation and cost-effectiveness.³¹ It is crucial to investigate algorithms that will process H-E images: computer-based systems compatible with daily clinical practice standards, such as H-E, may support the regular diagnostic procedure followed by pathologists as an objective, second-opinion tool.⁴⁻³²

Many previous studies considered methods based on the Hough transform,^{3,11,14,15} which requires accurate a priori knowledge of nuclear shape and size to optimize its performance. In these studies, the authors assumed an elliptical nuclear shape along with controlled variability in nuclear size. However, it has been reported that nuclear size and shape may vary significantly in high grade tumors. This variability is an indication of nuclear pleomorphism, a well-established diagnostic clue²⁹ and important indicator of the degree of tumor abnormality.³⁰ Thus, computer-based systems employing segmentation algorithms that experience difficulties in recognizing elongated, irregular-shaped and extremely small and large nuclei^{3,11,14,15,28} heighten the stakes for rejecting important diagnostic and prognostic information that is encoded as variability in the size and shape of nuclei. In contrast to these studies, the segmentation algorithm proposed above makes no assumptions about size, shape or texture of nuclei.

In Figure 4, small clumps of white pixels can be observed within the background. These are pixels erroneously detected as belonging to the nuclear cluster by the SVM algorithm. However, this is a result of the complicated targeting behavior of the H-E staining process. The H-E complex does not specifically target nuclei but concentrates in a variety of structures within surrounding tissue²; this targeting behavior results in highly textured images that complicate interpretation without providing additional diagnostic information.⁴ Elimination of these problematic regions was performed by size and fill holes filtering (Figure 5). The application of these filters did not affect nuclei shape. There also existed cases with fused or overlapped nuclei (Figure 8), which were incorrectly recognized as 1 structure by the algorithm.

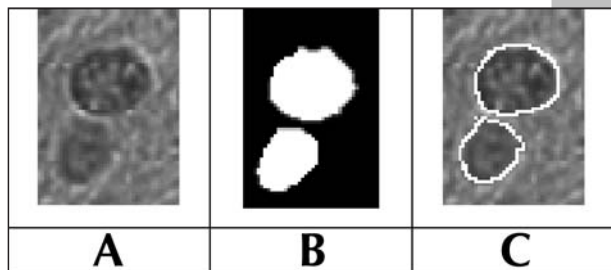


Figure 9 (A) Nuclei from H-E-stained biopsy of astrocytomas. (B) Resulting binary image after applying the SVMC pixel-based classification algorithm. (C) Final localization of nuclear boundaries.

The urinary bladder image in Figure 7 was selected to demonstrate performance of the proposed algorithm in cases where nucleoli exist. The arrow in Figure 7 indicates an incorrectly outlined nucleus by SVMC due to the existence of highly textured nucleoli. This could be a serious problem for the algorithm, as enlarged nucleoli are a very important and frequent diagnostic clue in dysplastic and malignant tissues. Therefore, we used the GVF active contour model to refine nuclear boundary detection. Figure 8 shows that after applying the GVF active contour model, nuclear boundaries were successfully detected. Figure 9 illustrates the whole procedure in the task of separating 2 closely located nuclei.

We developed a novel methodology for the automated segmentation of nuclear images combining SVMC and active contour models. The reason for developing and applying these demanding algorithms (SVMC and GVF) was that simple morphologic filters did not work satisfactorily in accordance with our histopathologists' opinions. The method was tested with 2 different types of routinely H-E-stained microscopic images. Results were evaluated by 2 histopathologists. The proposed method could be of value for computer-based systems aiming at interpreting microscopic images.

References

- DeAngelis LM: Brain tumors. *N Engl J Med* 2001;344:114-123
- Van de Wouwer G, Weyn B, Scheunders P, Jacob W, Van Marck E, Van Dyck D: Wavelets as chromatin texture descriptors for the automated identification of neoplastic nuclei. *J Microsc* 2000;97:25-35
- Spyridonos P, Cavouras D, Ravazoula P, Nikiforidis G: A Computer-based diagnostic and prognostic system for assessing urinary bladder tumour grade and predicting cancer recurrence. *Med Informat Internet Med* 2002;27:111-122
- Mouroutis T, Roberts, SJ Bharath AA: Robust cell nuclei segmentation using statistical modelling. *Bioimaging* 1998;6:79-91
- Wu H-S, Barba J: An efficient semi-automatic algorithm for cell contour extraction. *J Microsc* 1995;179:270-276
- Rosenthal DL, Acosta D, Peters RK: Computed-assisted re-screening of clinically important false negative cervical smears using the PAPNET testing system. *Acta Cytol* 1996;40:120-126
- Lie W: Automatic target segmentation by locally adaptive image thresholding. *IEEE Trans Image Proc* 1995;4:1036-1041
- Canny J: Computational approach to edge detection. *IEEE Trans Pattern Anal Machine Intell* 1986;PAMI-8:679-698
- Wu HS, Barba J: An algorithm for noisy cell contour extraction via area merging. *J Imaging Sci Technol* 1994;38:604-607
- Spyridonos P, Cavouras D, Ravazoula P, Nikiforidis G: Neural network based segmentation and classification system for the automatic grading of histological sections of urinary bladder carcinoma. *Analyt Quant Cytol Histol* 2002; 26:317-324
- Wu H-S, Barba J, Gil J: A parametric fitting algorithm for segmentation of cell images. *IEEE Trans Biomed Eng* 1998;45: 400-407
- Metzler V, Bredno J, Lehmann T, Spitzer K: A deformable membrane for the segmentation of cytological samples. *Proc SPIE* 1998;3338:1246-1257
- Lee K-M, Street N: An adaptive resource-allocating network for automated detection, segmentation and classification of breast nuclei topic area: image processing and recognition. *IEEE Trans Neural Networks* 2003;14:680-687
- Lee K-M, Street N: Automatic image segmentation and classification using on-line shape learning. *Proc of Workshop on Applications of Computer Vision, 2000*, pp 64-70
- Bamford P, Lovell B: Unsupervised cell nucleus segmentation with active contours models. *Signal Proc* 1998;71:203-213
- Mallat SG: A theory for multiresolution signal decomposition: The wavelet representation. *IEEE Trans Pattern Anal Machine Intell* 1989;11:674-693
- Ben-Hur A, Horn D, Siegelmann HT, Vapnik V: Support vector machine clustering. *J Machine Learning Res* 2001;2:125-137
- Faugeras O, Pratt W: Decorrelation methods of texture feature extraction. *IEEE Trans Pattern Anal Machine Intell* 1980;PAMI-2-14:323-332
- Parzen E: On the estimation of a probability density function and the mode. *Ann Math Stat* 1962;33:1065-1076
- Mahalanobis P: On the generalized distance in statistics. *Proc of National Institute of Science of India* 1936;00:49-55
- <http://www.cs.tau.ac.il/~borens/courses/ml/main.html>
- Gonzalez R, Woods R: Some basic morphological algorithms. *Digital Image Proc* 2002;00:534-547
- Gonzalez R, Woods R: Image segmentation. *Digital Image*

- Proc 2002;00:567–577
24. Xu C, Prince JL: Snakes, shapes, and gradient vector flow. *IEEE Trans Image Proc* 1998;00:359–369
 25. <http://iacl.ece.jhu.edu/projects/gvf/>
 26. Lee K-M, Street N: A fast and robust approach for automated segmentation of breast cancer nuclei. *Proc of Second IASTED International Conference on Computer Graphics and Imaging* 1999, pp 42–47
 27. McKenna SJ: Automated analysis of Papanicolaou smears. Ph.D. Thesis University of Dundee, 1994.
 28. MacAulay C, Palcic B: An edge relocation segmentation algorithm. *Analyt Quant Cytol Histol* 1989;12:165–171
 29. Scarpelli M, Montironi R, Thompson D, Bartels P: Computer-assisted discrimination of glioblastomas. *Analyt Quant Cytol Histopathol* 1997;19:369–375
 30. Coons W, Johnson P, Sceithauer B, Yates A, Pearl D: Improving diagnostic accuracy and interobserver concordance in the classification and grading of Primary Gliomas. *Cancer* 1997;79:1381–1393
 31. Bancroft J, Stevens A: *Theory and Practice of Histological Techniques*, 1990
 32. Glotsos D, Spyridonos P, Petalas P, Cavouras D, Ravazoula I, Dadioti P, Lekka I, Nikiforidis G: Supporting the regular diagnostic procedure followed by the experts in astrocytomas malignancy grading by means of an automatic classification methodology using support vector machines. *Analyt Quant Cytol Histol* 2004;26:77–83
 33. Giaretti AW, Gais P, Jütting U, Rodenacker K, Dörmer P: Correlation between chromatin morphology as derived by digital image analysis and autoradiographic labeling pattern. *Analyt Quant Cytol Histol* 1983;5:79–89
 34. Rodenacker K, Jütting U, Gais P, Burger G: Automatical image analysis in cytopathology. *Acta Stereol (suppl I)* 1983; 2:125–128
 35. Aubele M, Burger G, Rodenacker K: Problems concerning the quality of DNA measurements on Feulgen-stained imprints: A study of five fixation techniques. *Analyt Quant Cytol Histol* 1994;16:226–232
 36. Brenner JF, Lester JM, Selles WD: Scene segmentation in automated histopathology: Techniques evolved from cytology automation. *Pattern Recogn* 1981;13:65–77